Chemical investigation of hassium (element 108)

Ch. E. Düllmann*†, W. Brüchle‡, R. Dressler†, K. Eberhardt§, B. Eichler†, R. Eichler†, H. W. Gäggeler*†, T. N. Ginter||, F. Glaus†, K. E. Gregorich||, D. C. Hoffman||¶, E. Jäger‡, D. T. Jost†, U. W. Kirbach||, D. M. Lee||, H. Nitsche||¶, J. B. Patin||¶, V. Pershina‡, D. Piguet†, Z. Qin#, M. Schädel‡, B. Schausten‡, E. Schimpf‡, H.-J. Schött‡, S. Soverna*†, R. Sudowe||, P. Thörle§, S. N. Timokhin☆, N. Trautmann§, A. Türler, A. Vahle††, G. Wirth‡, A. B. Yakushev☆ & P. M. Zielinski||**

** Departement für Chemie und Biochemie, Universität Bern, CH-3012 Bern, Switzerland*
† Labor für Radio- und Umweltchemie, Paul Scherrer Institut, CH-5232 Villigen, Switzerland
‡ Gesellschaft für Schwerionenforschung mbH, D-64291 Darmstadt, Germany
§ Institut für Kernchemie, Universität Mainz, D-55128 Mainz, Germany
|| Nuclear Science Division, Lawrence Berkeley National Laboratory, Berkeley, California 94720, USA
¶ Department of Chemistry, University of California, Berkeley, California 94720-1460, USA
 # Institute of Modern Physics, Chinese Academy of Sciences, Lanzhou 730000, P.R. China
☆ Flerov Laboratory of Nuclear Reactions, Joint Institute for Nuclear Research, 141980 Dubna, Russia
*** Institut für Radiochemie, Technische Universität München, D-85748 Garching, Germany*
†† Research Center Rossendorf e.V., D-01314 Dresden, Germany

The periodic table provides a classification of the chemical properties of the elements. But for the heaviest elements, the transactinides, this role of the periodic table reaches its limits because increasingly strong relativistic effects on the valence electron shells can induce deviations from known trends in chemical properties[1–4]. In the case of the first two transactinides, elements 104 and 105, relativistic effects do indeed influence their chemical properties[5], whereas elements 106 and 107 both behave as expected from their position within the periodic table[6,7]. Here we report the chemical separation and characterization of only seven detected atoms of element 108 (hassium, Hs), which were generated as isotopes ^{269}Hs (refs 8, 9) and ^{270}Hs (ref. 10) in the fusion reaction between ^{26}Mg and ^{248}Cm. The hassium atoms are immediately oxidized to a highly volatile oxide, presumably HsO_4, for which we determine an enthalpy of adsorption on our detector surface that is comparable to the adsorption enthalpy determined under identical conditions for the osmium oxide OsO_4. These results provide evidence that the chemical properties of hassium and its lighter homologue osmium are similar, thus confirming that hassium exhibits properties as expected from its position in group 8 of the periodic table.

The discovery of Hs was reported in 1984 (ref. 11) with the identification of the nuclide ^{265}Hs with a half-life of $T_{1/2} = 1.5$ ms (refs 11, 12). In 1996, the much longer-lived isotope ^{269}Hs, with a half-life of about 10 s, was observed in the α-decay chain of ^{277}112 (ref. 8). Recently, evidence for the existence of the neighbouring nuclide ^{270}Hs was found and a half-life of about 4 s was deduced from its measured α-decay energy[10]. The latter two Hs isotopes might be sufficiently long-lived to allow their chemical characterization. Suitable reactions for their direct production are ^{248}Cm(^{26}Mg, 5,4n)^{269,270}Hs, for which formation cross-sections of a few picobarn have been estimated[13].

The periodic table suggests that Hs is a member of group 8 and thus chemically similar to its lighter homologues ruthenium (Ru) and osmium (Os), which are known to form highly volatile tetroxides. Therefore, Hs is also expected to form a very volatile tetroxide (HsO_4) suitable for gas-phase isolation[1,14–16], even though two earlier attempts to chemically identify Hs in the tetroxide form proved unsuccessful[17,18].

Fully relativistic density functional calculations[19] for the tetroxides of the group 8 elements indicated that the electronic structure of HsO_4 is very similar to that of OsO_4, with covalent bonding being somewhat more pronounced in the former. The stability of the gaseous tetroxides was found[19] to increase in the order $RuO_4 < OsO_4 < HsO_4$, in agreement with extrapolations within group 8 of the periodic table[20]. The density functional calculations, in conjunction with a surface interaction model, suggest adsorption

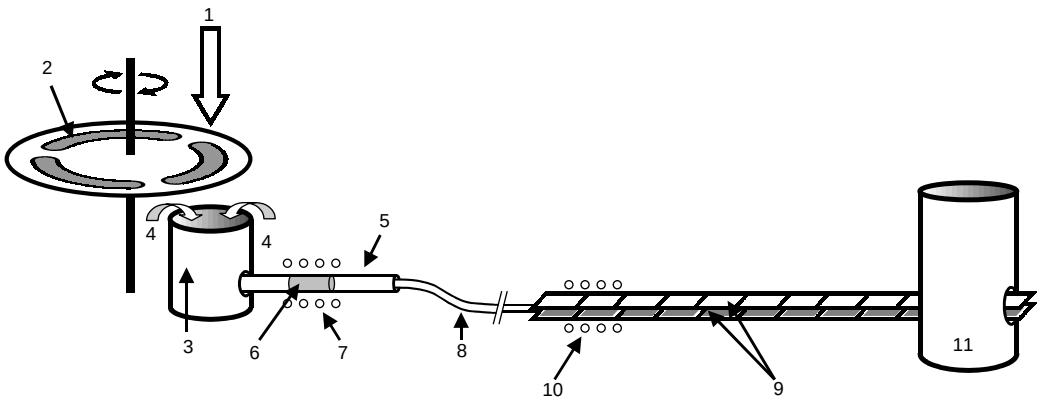

Figure 1 Schematic drawing of the IVO-COLD set-up used to produce and isolate Hs isotopes in form of the volatile HsO_4. The ^{26}Mg-beam (1) passes through the rotating vacuum window and ^{248}Cm-target (2) assembly. The target consisted of three banana-shaped segments (1.9 cm^2 area each) covered with 239 μg cm^{-2}, 730 μg cm^{-2}, and 692 μg cm^{-2} ^{248}Cm, respectively. The ^{248}Cm (isotopic composition ^{246}Cm: 4.2%; ^{248}Cm: 95.8%) was deposited on 2.82 mg cm^{-2} beryllium (Be) backings by molecular plating. The target-window assembly rotated in the adjacent gas volume with 2,000 rev min^{-1} and was synchronized with the beam macrostructure of the accelerator in order to distribute each 6-ms beam pulse evenly over one target segment. In the fusion reaction ^{269,270}Hs nuclei are formed that recoil out of the target into a gas volume (3) and are flushed with a He/O_2 mixture (4) out of the chamber. The gas was passed through a cartridge containing P_2O_5 as a drying agent before injecting it into IVO. In this way, the water vapour concentration was reduced to a measured value of <1 p.p.m. throughout the experiment. The gas was injected into a quartz column (5) containing a quartz wool plug (6) heated to 600 °C by an oven (7). There, Hs is converted to HsO_4 which is volatile at room temperature and transported with the gas flow through a 10-m-long perfluoroalkoxy (PFA) Teflon capillary (8) to the COLD detector array registering the nuclear decay (α and spontaneous fission) of the Hs nuclides. The array consists of 24 detectors arranged in 12 pairs (9). A temperature gradient was established along the detector array by means of a thermostat (10) at the entrance and a liquid nitrogen cryostat (11) at the exit. The temperature was monitored by five thermocouples installed along the copper bar. Depending on the volatility of HsO_4, the molecules adsorb at a characteristic temperature.

enthalpies of HsO_4 and OsO_4 on a quartz surface of $(-35.9 \pm 1.5)\,kJ\,mol^{-1}$ and $(-38.0 \pm 1.5)\,kJ\,mol^{-1}$, respectively. Extrapolations of the volatility of group 8 tetroxides suggest almost identical adsorption enthalpies of $(-46 \pm 15)\,kJ\,mol^{-1}$ and $(-45 \pm 15)\,kJ\,mol^{-1}$ for HsO_4 and OsO_4, respectively, whereas a physisorption model yields identical values of $(-47 \pm 11)\,kJ\,mol^{-1}$ for both tetroxides. Overall, the theoretical values suggest fairly similar adsorption behaviour for HsO_4 and OsO_4 on quartz. Although the present experiment uses detectors covered with a silicon nitride layer, we expect a direct analogy between theory and experiment because we observed comparable adsorption interactions of OsO_4 with quartz and silicon nitride.

The expected high volatility of group 8 tetroxides allows excellent separation from heavy actinides and lighter transactinides as well as from Pb, Bi and Po, which is important because several isotopes of these elements are formed with high yield as byproducts of the nuclear fusion reaction. These nuclides often decay via emission of α-particles and, therefore, severely interfere with the unambiguous detection of the nuclear decay of the investigated Hs nuclide.

Online investigations of Os oxides have already been conducted earlier[15,21,22]. Using the *in situ* volatilization and online detection apparatus (IVO) carrier-free $^{173}OsO_4$ ($T_{1/2} = 22.4$ s) could be separated and detected with an overall efficiency of (40 ± 10)%. Decontamination from Po ($\geq 2 \times 10^4$) was excellent[21].

The experimental set-up, schematically shown in Fig. 1, involves mounting the ^{248}Cm target[23] on a rotating wheel and bombarding it with up to 8×10^{12} $^{26}Mg^{5+}$ particles per second, delivered by the UNILAC accelerator at the Gesellschaft für Schwerionenforschung mbH. The particle beam first passed through a rotating three-segment $3.68\,mg\,cm^{-2}$ Be vacuum window which allowed for a pressure up to 1.3 atm in the recoil chamber. The 192.7-MeV beam energy delivered by the UNILAC resulted in ^{26}Mg projectile energies of 143.7–146.8 MeV inside the ^{248}Cm target. Nuclear reaction products recoiling from the target were thermalized in the gas volume (34 ml) of the IVO device[21] flushed with dry (measured water vapour concentration <1 p.p.m.) $1.2\,l\,min^{-1}$ helium (He) and $100\,ml\,min^{-1}$ oxygen (O_2). The reaction products were transported with the carrier gas through a 30-cm-long quartz column (internal diameter, i.d., 4 mm) containing a quartz wool plug at a distance of 6.5 cm from the recoil chamber. This plug was heated to 600 °C and served as a filter for aerosol particles and provided a surface to complete the oxidation reaction of Os and Hs to their tetroxides, which were further transported through a 10-m-long perfluoroalkoxy (PFA) Teflon capillary (i.d., 2 mm) to the detection system. The capillary was installed inside a polyamide (PA) tube flushed with dry N_2.

Using gas phase adsorption thermochromatography[24], we measured the temperature at which HsO_4 deposits, with a chromatographic column along which a stationary negative temperature gradient is maintained. The chromatographic column, the cryo online detector (COLD), also served as detection system for the identification of decaying atoms of $^{269,270}Hs$. COLD consists of 12 pairs of silicon PIN-photodiodes of $1 \times 3\,cm^2$ active area mounted at a distance of 1.5 mm via two spacers made from silicon. PIN diodes are well suited for detection of α-particles or fission fragments. The diode pairs were installed inside a copper bar. A temperature gradient from −20 °C to −170 °C was established along the detector array. The efficiency for detecting a single α-particle emitted by a species adsorbed within the detector array was 77%. To avoid formation of ice layers on the detector surfaces, the whole device was placed inside a vacuum tight housing flushed with dry N_2. COLD is an improved version of a previous set-up called the cryo-thermochromatography separator (CTS)[22].

The detectors of the COLD array were online calibrated with α-decaying ^{219}Rn and its daughters ^{215}Po and ^{211}Bi using a ^{227}Ac source. The determined energy resolution was 50–70 keV (full-

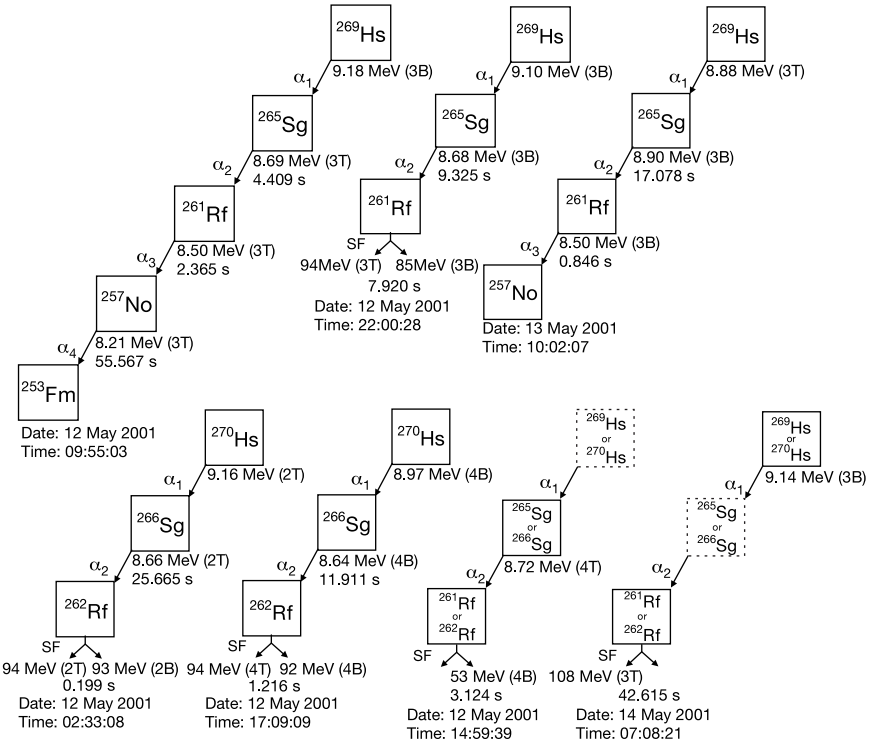

Figure 2 The seven nuclear decay chains originating from Hs isotopes that were detected in the course of the experiment permit an unambiguous identification of hassium after chemical separation. Indicated are the energies of α-particles and fission fragments in megaelectronvolts (MeV) and the lifetimes in seconds (s). The detector in which the decay was registered is indicated in parentheses where T stands for top detector and B for bottom detector. For each chain the date and time of its registration are given. The lifetime of the mother isotope could not be determined with the applied thermochromatography technique because the deposition time is not measured.

width at half-maximum, FWHM) for detectors 1 through 8 and 80–110 keV (FWHM) for detectors 9 through 12.

The proper functioning of the IVO-COLD system was checked at the beginning and after the end of the Hs experiment by mounting a 800 $\mu g\,cm^{-2}$ ^{152}Gd (32% enriched) target to produce short-lived Os isotopes in the reaction $^{152}Gd(^{26}Mg, 6n)^{172}Os$. The beam intensity was $1 \times 10^{12}\,s^{-1}$ and the beam energy in the middle of the target 153 MeV. All other experimental parameters, including gas composition and flow rate, were identical to those of the Hs experiment. In the COLD detector array the α-decay of ^{172}Os was registered. ^{172}Os has a half-life of 19.2 s and a 1.0% α-decay branch with $E_\alpha = 5.10$ MeV.

The experiment to produce Hs isotopes lasted 64.2 h during which a total of 1.0×10^{18} ^{26}Mg particles passed through the target. Only α-lines originating from ^{211}At, $^{219,220}Rn$ and their decay products were identified. Whereas ^{211}At and its decay product ^{211}Po were deposited mainly in the first two detectors, $^{219,220}Rn$ and their decay products accumulated in the last three detectors, where the temperature was sufficiently low to partly adsorb Rn. One side of detector pair 1 did not operate owing to a technical failure and, therefore, this detector unit was excluded from the data analysis. During the experiment, seven correlated decay chains were detected (see Fig. 2). All correlated α-decay chains were observed in detectors 2 through 4 and assigned to the decay of ^{269}Hs or ^{270}Hs. The characteristics of the first three decay chains agree well with data[8,9] on ^{269}Hs and its daughter nuclides, while two other decay chains can be attributed[10] to the decay of ^{270}Hs. The last two decay chains were incomplete and a definite assignment to ^{269}Hs or ^{270}Hs could not be made. No additional three-member decay chains within ≤300 s were registered in detectors 2 to 10. The background count-rate of α-particles with energies between 8.0 and 9.5 MeV was about $0.6\,h^{-1}$ per detector, leading to very low probabilities of $\leq 7 \times 10^{-5}$ and $\leq 2 \times 10^{-3}$ for any of the first five chains and any of the last two chains, respectively, being of random origin. In addition, four uncorrelated fission fragments with energies >50 MeV were registered in detectors 2 through 4. All other detectors registered no fission fragments, except for one fission fragment being observed in the operating side of detector 1.

As depicted in Fig. 3, the α-decay of one Hs atom was registered in detector 2, the decay of four atoms in detector 3 and the decay of two atoms in detector 4. The maximum of the Hs distribution was found for a temperature of (-44 ± 6) °C. The deposition distribution of OsO_4 measured before and after the experiment revealed a maximum in detector 6 at (-82 ± 7) °C.

The adsorption enthalpy (ΔH_{ads}) of the compound on the stationary phase is extracted from the measured deposition distribution by using Monte Carlo simulations of the trajectories of single molecules as they move along the column under real experimental conditions[25]. The only free parameter in the simulations is ΔH_{ads}, but the half-life of the nuclide is a crucial parameter. For this reason, and because the half-life of ^{270}Hs has not yet been measured, only decays assigned to ^{269}Hs were used to evaluate the adsorption enthalpy of the compound on the silicon nitride surface. The results that best reproduce the experimental data are shown in Fig. 3 (solid lines) and suggest a value of $\Delta H_{ads} = (-46 \pm 2)\,kJ\,mol^{-1}$ (68% confidence interval, c.i.), which was inferred using a $T_{1/2}$ value of 11^{+15}_{-4} s for ^{269}Hs (refs 8, 9). The given uncertainty is the total uncertainty; that is, it reflects the width of the measured deposition peak and the uncertainty in $T_{1/2}$. The adsorption enthalpy of OsO_4 on silicon nitride deduced from this experiment was $(-39 \pm 1)\,kJ\,mol^{-1}$, which is in good agreement with the adsorption enthalpy obtained in earlier investigations using quartz surfaces[15,21,22].

The experimentally derived adsorption enthalpy of HsO_4 is thus lower than that of OsO_4, while the predictions suggest either similar values[20] or a slightly higher value[19] for HsO_4. However, the theoretical values and experimental values have associated uncertainties. Moreover, the low value of the ΔH_{ads} determined for the hassium oxide species clearly suggests that it is HsO_4, given that, by analogy with the known properties of the Os oxides, other Hs oxides are all expected to be less volatile and unable to reach the detection system. The observed formation of a very volatile Hs molecule, presumably HsO_4, in a mixture of oxygen and helium thus provides strong qualitative evidence that Hs is an ordinary member of group 8 of the periodic table that behaves similarly to its lighter homologue Os. □

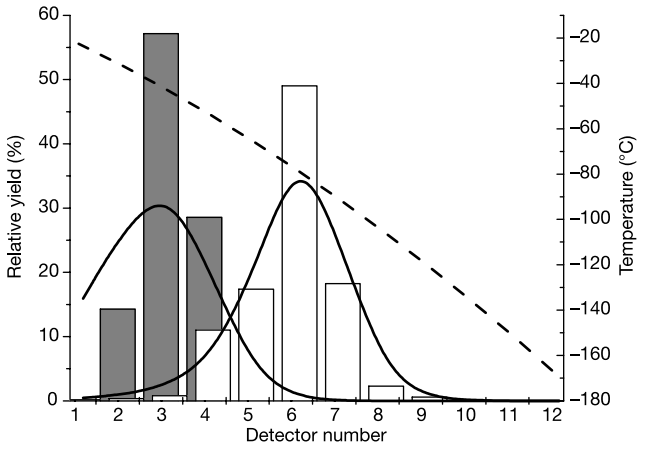

Figure 3 Merged thermochromatogram of HsO_4 and OsO_4. Indicated are the relative yields of HsO_4 and OsO_4 for each of the 12 detector pairs. Measured values are represented by bars: HsO_4, dark grey; OsO_4, white. For Hs, the following distribution was measured: ^{269}Hs: three events (all in detector 3); ^{270}Hs: two events (one in detector 2 and one in detector 4); Hs (isotope unknown): two events (one in detector 3 and one in detector 4). For Os, the distribution of 1×10^5 events of $^{172}OsO_4$ is given. The dashed line indicates the temperature profile (right-hand scale). The maxima of the deposition distributions were evaluated as (-44 ± 6) °C for HsO_4 and (-82 ± 7) °C for OsO_4 where the uncertainties indicate the temperature range covered by the detector which registered the maximum of the deposition distribution. Solid lines represent results of a Monte Carlo simulation of the migration process of the species along the column with standard adsorption enthalpies of $-46.0\,kJ\,mol^{-1}$ for $^{269}HsO_4$ and $-39.0\,kJ\,mol^{-1}$ for $^{172}OsO_4$.

Received 8 April; accepted 9 July 2002; doi:10.1038/nature00980.

1. Fricke, B. Superheavy elements. *Struct. Bonding* **21,** 90–144 (1975).
2. Pyykkö, P. & Desclaux, J.-P. Relativity and the periodic system of elements. *Acc. Chem. Res.* **12,** 276–281 (1979).
3. Pershina, V. G. Electronic structure and properties of the transactinides and their compounds. *Chem. Rev.* **96,** 1977–2010 (1996).
4. Schwerdtfeger, P. & Seth, M. Relativistic effects of the superheavy elements. *Encyclopedia of Computational Chemistry* Vol. 4 2480–2499 (Wiley, New York, 1998).
5. Kratz, J. V. in *Heavy Elements and Related New Phenomena* Ch. 4 (eds Greiner, W. & Gupta, R. K.) 129–193 (World Scientific, Singapore, 1999).
6. Schädel, M. *et al.* Chemical properties of element 106 (seaborgium). *Nature* **388,** 55–57 (1997).
7. Eichler, R. *et al.* Chemical characterization of bohrium (element 107). *Nature* **407,** 63–65 (2000).
8. Hofmann, S. *et al.* The new element 112. *Z. Phys. A* **354,** 229–230 (1996).
9. Hofmann, S. & Münzenberg, G. The discovery of the heaviest elements. *Rev. Mod. Phys.* **72,** 733–767 (2000).
10. Türler, A. *et al.* Decay properties of ^{269}Hs and evidence for the new nuclide ^{270}Hs. *Eur. Phys. J. A* (submitted).
11. Münzenberg, G. *et al.* The identification of element 108. *Z. Phys. A* **317,** 235–236 (1984).
12. Hofmann, S. *et al.* Production and decay of $^{269}110$. *Z. Phys. A* **350,** 277–280 (1995).
13. Schädel, M. & Hofmann, S. Prospects for the discovery of new elements. *J. Radioanal. Nucl. Chem.* **203,** 283–300 (1996).
14. Bächmann, K. & Hoffmann, P. Chemische Probleme bei der Darstellung überschwerer Elemente durch Kernreaktionen. *Radiochim. Acta* **15,** 153–163 (1971).
15. Domanov, V. P. & Zvara, I. Continuous-flow thermochromatographic separation of unsupported radioisotopes of platinum elements in a stream of air from nuclear reaction products in an accelerator heavy-ion beam. *Sov. Radiochem.* **26,** 731–739 (1985); translated from *Radiokhimiya* **26,** 770–778 (1984).
16. Zude, F., Fan, W., Trautmann, N., Herrmann, G. & Eichler, B. Thermochromatography of platinum elements in oxygen: Radiochemical studies of the behaviour of rhodium, palladium, osmium and platinum. *Radiochim. Acta* **62,** 61–63 (1993).
17. Zhuikov, B. L., Kruz, H. & Zvara, I. Possibilities of chemical identification of short-lived isotopes of

element 108. Report P7-86-322, page 26 (Joint Institute for Nuclear Research, JINR, Dubna, 1986) (in Russian).
18. Dougan, R. J., Moody, K. J., Hulet, E. K. & Bethune, G. R. OSCAR: An apparatus for on-line gas-phase separations. FY87 Annual Report UCAR 10062/87, 4–17 (Lawrence Livermore National Laboratory, LLNL, Nuclear Chemistry Division, Livermore, 1987).
19. Pershina, V., Bastug, T., Fricke, B. & Varga, S. The electronic structure and properties of group 8 oxides MO_4, where M = Ru, Os, and element 108, Hs. *J. Chem. Phys.* **115,** 792–799 (2001).
20. Düllmann, Ch. E., Eichler, B., Eichler, R., Gäggeler, H. W. & Türler, A. On the stability and volatility of group 8 tetroxides MO_4 (M = ruthenium, osmium, and hassium (Z = 108)). *J. Phys. Chem. B* **106,** 6679–6684 (2002).
21. Düllmann, Ch. E. *et al.* IVO, a device for in situ volatilization and on-line detection of products from heavy ion reactions. *Nucl. Instrum. Meth.* A **479,** 631–639 (2002).
22. Kirbach, U. W. *et al.* The cryo-thermochromatographic separator (CTS): A new rapid separation and α-detection system for on-line chemical studies of highly volatile osmium and hassium (Z = 108) tetroxides. *Nucl. Instrum. Meth.* A **484,** 587–594 (2002).
23. Malmbeck, R. *et al.* Separation of ^{248}Cm from a ^{252}Cf neutron source for production of Cm targets. *Radiochim. Acta* **89,** 543–549 (2001).
24. Zvara, I. Thermochromatographic method of separation of chemical elements in nuclear and radiochemistry. *Isotopenpraxis* **26,** 251–258 (1990).
25. Zvara, I. Simulation of thermochromatographic processes by the Monte Carlo method. *Radiochim. Acta* **38,** 95–101 (1985).

Acknowledgements

We thank the staff of the Laboratory for Micro- and Nanotechnology at PSI for manufacturing the PIN-diode sandwiches for the COLD array and the staff of the GSI UNILAC for providing stable, highly intense beams of ^{26}Mg as well as the target laboratory for Be foils for the vacuum windows. Support from the European Commission Institute for Transuranium Elements, Karlsruhe, for long-term storage of ^{252}Cf and the chemical separation of ^{248}Cm is appreciated. These studies were supported in part by the Swiss National Science Foundation and the Chemical Sciences Division of the Office of Basic Energy Sciences, US Department of Energy.

Competing interests statement

The authors declare that they have no competing financial interests.

Correspondence and requests for materials should be addressed to H.W.G. (e-mail: gaeggeler@iac.unibe.ch).

Mantle compensation of active metamorphic core complexes at Woodlark rift in Papua New Guinea

Geoffrey A. Abers*, Aaron Ferris*, Mitchell Craig†‡, Hugh Davies†, Arthur L. Lerner-Lam§, John C. Mutter§ & Brian Taylor‖

* *Department of Earth Sciences, Boston University, Boston, Massachusetts 02215, USA*
† *Department of Geology, University of Papua New Guinea, Port Moresby, Papua New Guinea*
§ *Lamont-Doherty Earth Observatory of Columbia University, Palisades, New York 10964, USA*
‖ *University of Hawaii, Manoa, Hawaii 96822, USA*

In many highly extended rifts on the Earth, tectonic removal of the upper crust exhumes mid-crustal rocks, producing metamorphic core complexes. These structures allow the upper continental crust to accommodate tens of kilometres of extension[1], but it is not clear how the lower crust and underlying mantle respond. Also, despite removal of the upper crust, such core complexes remain both topographically high and in isostatic equilibrium. Because many core complexes in the western United States are underlain by a flat Moho discontinuity[2,3], it has been widely assumed that their elevation is supported by flow in the lower crust[4–6] or by magmatic underplating[7]. These processes should decouple upper-crust extension from that in the mantle. In contrast, here we present seismic observations of metamorphic core complexes of the western Woodlark rift that show the overall crust to be thinned beneath regions of greatest surface extension. These core complexes are actively being exhumed[8] at a rate of 5–10 km Myr^{-1}, and the thinning of the underlying crust appears to be compensated by mantle rocks of anomalously low density, as indicated by low seismic velocities. We conclude that, at least in this case, the development of metamorphic core complexes and the accommodation of high extension is not purely a crustal phenomenon, but must involve mantle extension.

The Woodlark rift of Papua New Guinea (Fig. 1) is the site of some of the youngest, most recently uplifted metamorphic core complexes (MCCs) on the planet[8], and the most rapidly extending continental crust[9]. Extension began producing new sea floor along strike by 5–6 Myr ago[10], leading to MCC exhumation on Fergusson and Goodenough islands in the Pliocene epoch, as indicated by sediment composition in adjacent basins[8]. Most workers infer that extension is driven by plate forces such as slab pull at other margins of the Solomon Sea[11] or by gravitational collapse[10], similar to some large-extension rifts elsewhere but contrasting with active rifts such as the east Africa rift[12,13]. Magnetic lineations require 100–200 km extension across the D'Entrecasteaux MCCs[10], at 20–35 mm yr^{-1}, much of which must be accommodated on the north-dipping detachment shear zones bounding them. The MCCs show rapid uplift, with footwall rocks having experienced conditions of 700–900 °C and 5–6 kbar as recently as 3–4 Myr ago, and 4–5 kbar at similar temperatures at 1.5–2 Myr ago[14,15]. The MCCs seem to be at present exhuming, as indicated by geomorphic[16] and low-temperature geochronological indicators[14].

In 1999 and 2000, we placed 19 broadband seismographs at 11 sites across the western Woodlark rift (Fig. 1), from the relatively unextended Papuan peninsula in the south, across the D'Entrecasteaux MCCs, to the northern edge of the Trobriand platform. Data recorded by these stations provide, to our knowledge, the first available constraints on the deep structure of this rift.

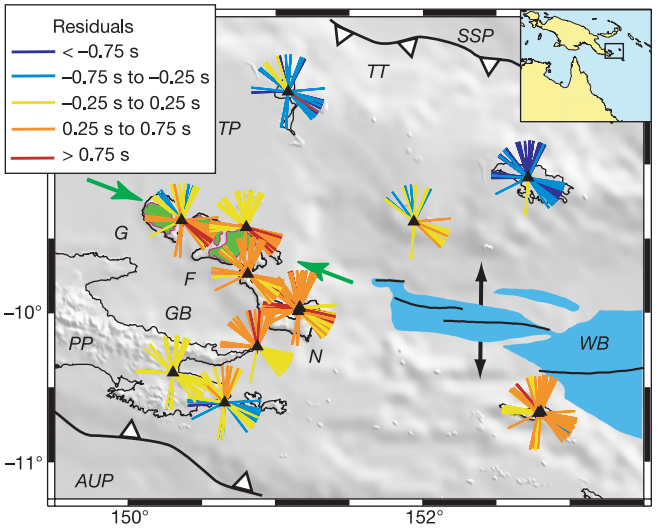

Figure 1 Tectonic features of the western Woodlark rift, showing seismic stations (small black triangles) and azimuths of incident teleseismic rays. Blue shaded region, new sea floor (<2 Myr old); black arrows, direction of modern extension; green arrows, chain of MCCs. Letters denote the D'Entrecasteaux islands: Goodenough (G), Fergusson (F) and Normanby (N); the Papuan peninsula (PP), Goodenough basin (GB), Trobriand platform (TP), Trobriand trough (TT), Woodlark basin (WB), Australian plate (AUP), and Solomon Sea plate (SSP). Lines radiating from stations point at back-azimuth of incident teleseismic P waves, and indicate travel time residuals by colour. Blue lines, indicating negative residuals, show seismically fast regions while red regions indicate slow regions.

‡ Present address: Department of Geological Sciences, California State University, Hayward, California 94542, USA.